Soft Robot Employing a Series of Pneumatic Actuators and Distributed Balloons: Modeling, Evaluation, and Applications

Tuan Tai Nguyen, *Student Member, IEEE*, Dinh Quang Nguyen, *Member, IEEE*, and Van Anh Ho, *Senior Member, IEEE*

***Abstract*—Tasks involving exploration and inspection of narrow environments demand a robot to have a flexible body. Such a robot is especially preferred if the integrity of its surrounding is crucial, as in endoscopy procedures. We propose the design of a small, self-propelled soft robot that can operate in a constrained environment. By periodic activation of a series of pneumatic actuators fabricated using a casting technique, sinusoidal locomotion is achieved. The wave-like locomotive strategy with an additional support mechanism enabled movement in multiple scenarios, including traveling horizontally and vertically in environments of different characteristics. Two analytical models are presented to highlight the design characteristics. The first predicts the velocity of the robot in relation to the working conditions, while the second calculates the force that the robot body exerts on its surroundings. Its mobility was tested in simple and complex routes under rigid and elastic environments. The resulting percent errors for the predictions of velocity and lateral force are 7.89% and 16.86%, respectively. In terms of performance, the robot can move horizontally in rigid tubes even if the walls are lubricated, and can achieve a peak speed of 40.11 mm/s, or 0.171 Body-Length/s (BL/s). With the addition of a tail balloon, the robot also successfully ascended a vertical tube with a maximum speed of 9.22 mm/s (or 0.039 BL/s). The presented work is expected to pave the way toward feasible robotic applications, such as pipe inspection.**

***Index Terms*—Inspection robot, pneumatic actuator, self-propelled robot, soft robotics.**

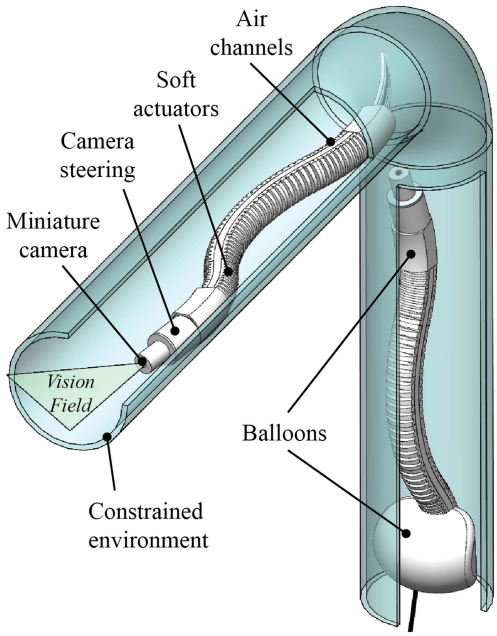

Fig. 1. Self-propelled soft robot is constructed from a series of pneumatic actuators and integrated with a miniature camera for inspection. Balloons are attached at two ends of the robot to support vertical locomotion and anchoring for inspection in vertical environments. Four-chamber soft steering is put behind the camera to enlarge the field of vision.

I. Introduction

BIO-INSPIRED robots, which mimic the abilities of animals, have attracted the interest of researchers in recent years as more applications involving interactions between robots and environments are emerging [1]. In nature, animals such as snakes and eels have long, cylindrical, body shapes, enabling them to slither along the ground, burrow underground, and swim underwater. Inspired by creatures, researchers have developed robots with locomotion abilities including walking [2], crawling [3], [4], and swimming [5], [6]. Studies have demonstrated that robots can perform complex and multiphase movement through challenging terrains including obstacles [7], [8], [9], [10]. Terrains including confined spaces like tunnels and caves pose a major challenge to robots in terms of their size and mobility. To tackle this challenge, cylindrical-shaped robots have been designed for tubular object inspection [11], [12], [13], [14], [15]. These worm-like designs omit mechanisms such as wheels or propellers to minimize the robot's cross-section allowing it to negotiate pipelines of different sizes with bends. With the incorporation of soft materials, the concept of such elongated robots may be applied in colonoscopy procedures [16], [17]. An optimum combination of material and design ensures gentle interaction between the robot and its surroundings, which is

Manuscript received 16 February 2024; revised 1 July 2024; accepted 10 July 2024. Date of publication 16 August 2024; date of current version 28 August 2024. This article was recommended for publication by Associate Editor B. Rosa and Editor A. Menciassi upon evaluation of the reviewers' comments. *(Tuan Tai Nguyen and Dinh Quang Nguyen contributed equally to this work.) (Corresponding author: Van Anh Ho.)*

Tuan Tai Nguyen and Van Anh Ho are with the Soft Haptics Lab., School of Materials Science, Japan Advanced Institute of Science and Technology, Ishikawa 923-1292, Japan (e-mail: van-ho@jaist.ac.jp).

Dinh Quang Nguyen is with the VNU University of Engineering and Technology, Ha Noi 123105, Vietnam.

Design and source code for this article are published at: https://github.com/Ho-lab-jaist/inspection-robot.git

This article has supplementary downloadable material available at https://doi.org/10.1109/TRO.2024.3444069, provided by the authors.

Digital Object Identifier 10.1109/TRO.2024.3444069

crucial in applications to deliver safe and painless procedures in patients.

In the present study, we designed and developed a self-propelled soft robot as depicted in Fig. 1, which may operate in both rigid and elastic tubular environments. To represent the latter environment, we envisaged an application for colonoscopy. The robot includes a series of soft pneumatic actuators controlled by multiple pulse signals at a suitable phase lag to create a dynamic sinusoidal posture. This results in a movement resembling wave propagation, enabling the robot to move back and forth through a complex narrow tubular route. The design includes balloons to support climbing movement, which effectively widens the workspace of the robot. Finally, a steering component attached to its head adjusts the angle of an onboard camera. The main contributions of this research are as follows:

1) Implement the design of a small, soft, self-propelled robot and its fabrication by casting/molding technique. The basic design was inspired by the work done in [18].
2) Proposal of a novel vertical locomotion, and anchoring strategy for the robot, thanks to deposited balloons.
3) Development of a velocity and reaction force model to estimate the performance of the robot using analytical approach.
4) Proposal of pilot experimental evaluation methods to validate the characteristics of the robot and effects of the input pressure, frequency, and environment, on its locomotion efficiency.
5) Open sourcing both hardware and software related to the development of this robot. Details can be seen at https://github.com/Ho-lab-jaist/inspection-robot.git

In Section II, we review related works. In Section III, inspired by preceding studies, the design of a 235 mm long self-propelled soft robot with control strategies for different terrains is described. Section IV discusses the modeling of velocity and exerted lateral force. Section V details a comprehensive series of experiments to evaluate models and the performance of the robot. Section VI presents the results. Section VII shows the robot's ability to travel in challenging environments. Section VIII discusses this research. Finally, Section IX concludes this article. Video for motion of the robot can be seen here: https://youtu.be/PwSEBtvPn48

II. Related Works

A. Inspection Robot for Tubular Objects

Many tubular objects exist as natural or manufactured structures such as human organs and fuel-transporting pipelines. The need to inspect inside small tubular objects, which are typically inaccessible to humans, presents opportunities for the development of a dedicated class of robots. Earlier robots of this field often included a rigid body combined with support mechanisms [19], [20], [21], [22], [23], [24], [25]. These designs usually comprised single or multiple compact units facilitating control and maneuverability. Use of extendable wheels [19], [20], [21] or legs [23], [25] enable robots to generate better traction to the pipe wall. In addition, due to the rigidity of component materials and the linear behavior of devices, their characterizations by mathematical modeling of interaction forces and moving speeds may be determined relatively easily while assuring accuracy. This is significantly beneficial in describing and predicting the performance of a robot, which gives an insightful understanding of governing physics. However, these robots encounter great challenges in navigating bends in narrow pipelines and risk damaging the structure of the object being explored. Furthermore, wheels and legs may become entangled or otherwise negatively interact with the surface features of soft, elastic terrains.

To overcome these environmental challenges and reduce the number of peripheral components of a robot, researchers designed robots of long, slim structures, whose bodies are directly used to achieve mobility. This type of robot, which requires a higher number of degree of freedom (DOF) for its body, also gives rise to the use of soft materials. Inspired by the movement of an inchworm, several designs composed of a main extensible body and clamping mechanisms have been proposed [12], [13], [14], [15]. The robot presented by Liu et al. [14] demonstrated the ability to vertically carry a weight of over 11-fold its own. In free climb, it reaches a velocity of 4.23 mm/s. Lin et al. [15] developed a McKibben actuator-based robot that could operate in horizontal or vertical pipes. It achieved a peak speed of 27 mm/s in horizontal locomotion. However, it was quite large and could not perform a 90° turn due to the McKibben actuator stiffness.

In contrast to a rigid, smooth, pipe, the work of an inspection robot might require navigating an elastic, irregular terrain, such as a colonoscopy procedure. Also utilizing the principle inspired by the inchworm, a soft robot was developed for colonoscopy by Manfredi et al. [16]. To provide anchorage in colon segments of different diameters, their robot employs two air-inflated balloons, which combine with a 3-DoF body to create forward movement and the ability to steer the vision of a housed camera. The robot completed a traveling distance of 1.4 m inside a phantom colon in 8 min 30 s. Another approach to colonoscopy robots was proposed by Bernth et al. [17]. Instead of using pneumatic clamping mechanisms, their robot anchored itself by bending one of its segments. The reported average velocity of this robot was 1.21 mm/s. Although the above designs show reliable locomotion capability, their speed is limited by the "anchor then elongate" movement based on an inchworm. Robotic colonoscopes employing treads driven by worm gear [26], [27], [28] achieved better performance in terms of speed. The capsule endoscopes presented by Formosa et al. [27] attained a high velocity of 40 mm/s inside a porcine colon.

As opposed to self-driven mechanisms, capsule colonoscopy robots can also be navigated using electromagnetic-based methods. Martin et al. [29] developed an intelligent and autonomous control of a magnetic flexible endoscope. This system employs a KUKA LBR Med robotic arm to guide the endoscope and allows nonexperts to perform magnetic colonoscopy with an average completion time of 17 min, corresponding to a speed of approximately 1.47 mm/s. Utilizing a similar principle, however, not having to rely on a robotic arm, Zhang et al. [30] introduced

a hand-held control panel for the navigation of the capsule robot that can reach a speed of 54 mm/s in a simulator. Nevertheless, the designs [26], [27], [28], [29], [30] were fabricated from mainly rigid materials and their ability to ascend an incline is limited due to the lack of mechanisms supporting climbing. Regarding another type of movement, Qi et al. [18] proposed a soft snake robot whose body consists of a series of pneumatic bending actuators. As air is pumped into the chambers, the robot deforms into a sinusoidal shape, which results in wave-like locomotion. This traveling method achieved an impressive top speed of 35 mm/s. However, its length of approximately 520 mm, since it was 3-D printed, limited its use in narrow spaces. Another drawback was the lack of vertical locomotion and a means to anchor the robot. Therefore, the need to design a small, fully functioning, and speedy inspection robot remains.

B. Modeling Methods

Modeling is essential to understand the physics and optimize the control strategy of a robot. Compared to traditional rigid robots whose movements can be described by six degrees of freedom, the movements of soft bodies theoretically need an infinite number of degrees of freedom for their explanation [31]. In the case of elongated robots, their postures resemble continuous curves, which are highly complex and require different approaches for each circumstance. In recent years, finite element-based models have been widely applied to structural problems. This approach has successfully simulated the behavior of actuators used in snake-like [18] and eel-like [32] robots. However, finite element analysis often demands great computational power, therefore, it is not suitable for real-time calculations. Another approach is analytical models [2], [6], [33], [34], [35], [36], [37], [38], [39], [40], [41], in which the physics can be simplified by selective assumptions resulting in fast and efficient calculations. Among these techniques, the Lagrangian method has been proven effective in application to a variety of designs. Akbarzadeh et al. [35] proposed a dynamics model, which is based on Lagrangian formulations, for the lateral undulation motion of a multilink snake robot. While the model gives a clear representation of each of the robot links and can calculate the joint torque in real time, it is only suitable for rigid and linear systems. The Lagrangian method shows potential in formulating a dynamic model for soft pneumatic actuators [42] applied in eel-inspired [6] and snake-inspired [18] robots. However, when the actuator moves rapidly and interacts with its environment, solving such differential equations poses several difficulties including complex constraint conditions and a significant increase in computational time. Nguyen and Ho [6] presented a geometry-based model for wave-like locomotion by an underwater eel robot. This approach expressed the shape of the robot by a sinusoidal function, resulting in simpler and faster calculations. A similar method was utilized by Zhao et al. [39] to describe the undulation locomotion of a snake robot in a confined space, however, a full evaluation was not reported. Although much effort has been made to explain the locomotion of elongated robots, a model accounting for constraints imposed by the environment has not been realized. In addition to assessing the efficacy of robotic motion, it is imperative to investigate the applied force exerted by the robot upon its surroundings. This particular aspect assumes paramount significance when operating in environments comprising fragile, delicate materials.

III. System Design

A. Robot's Design and Fabrication

Robots with soft elongated bodies can employ a series of pneumatic actuators controlled by pulse signals with shifting phases that create propagation waves from head to tail to move [6], [18], [36]. In these designs, actuators on opposite sides of the body are activated independently by pressurized air sources to create flapping movements. The robot structure and operating principle provide potential for locomotion in constrained spaces without support mechanisms such as wheels or legs. Based on previous studies, here we implement a design for a self-propelled soft robot, inspired by the work done in [18], with a series of soft actuators with a structure appropriate for fabrication by *casting* technique.

The robot's main body comprises multiple air chambers attached to both sides of a soft air path. Running through the air path are four air channels that supply air to create undulatory movement. Along the air path, air windows are arranged to distribute pressurized air from the air channels to corresponding air chambers so the robot adopts a sinusoidal wave-like posture. In the middle of the air path is a tunnel housing a miniature cable camera whose angle is adjusted by a pneumatic steering component with four air chambers which can bend and point the robot head in four directions. Different to the design in [18], two balloons, attached to the head and tail of the robot, assist in anchoring and vertical climbing, respectively. The head balloon is inflated to fix the robot in position. In contrast, the tail balloon can only be inflated on one side. This asymmetry is intentional to avoid impeding the robot's ability to adopt a wave-like posture.

To construct the robot, a series of molds were designed using 3-D CAD software SOLIDWORKS (Dassault Systèmes, France) and printed by a 3-D printer (Prusa i3 MK3S+, Prusa Research, Czech Republic). The main steps of the fabrication process after obtaining the molds are described in Fig. 2:

1) Step 1: Several types of Dragon Skin liquid silicone rubber (Smooth-On, Inc., USA), which provide appropriate stiffness for different components of the robot, were chosen. Dragon Skin 30 was used to fabricate the air path and air chambers, and Dragon Skin 10 for the balloons and camera steering. After mixing parts A and B of the silicone, it was poured into the molds, cured at room temperature for 4 h, then the components were removed.
2) Step 2: The robot components were glued together using Dragon Skin 30. An ultra-tiny camera with integrated LED (MD-V2000LH-120, Misumi Electronic Corporation, Taiwan) was inserted through the middle channel of the robot. Several silicone air tubes were attached to the tails of the air channels.

Assembly from component pieces allows for different robot body lengths to suit working environments. For the application of colonoscopy robot, we decided the length of the robot body

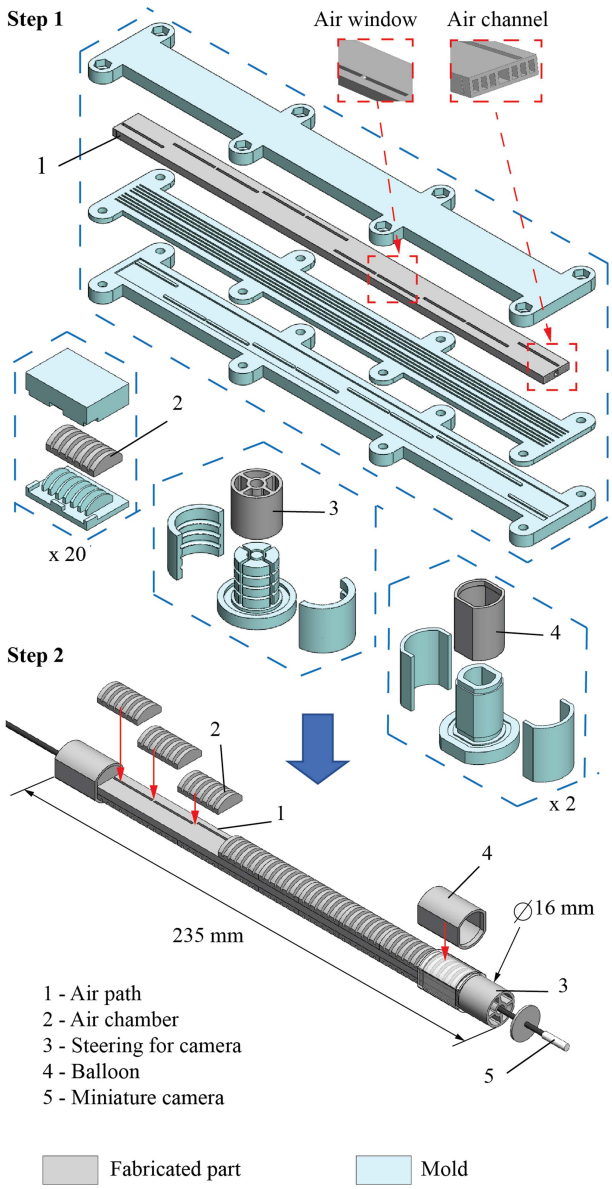

Fig. 2. Design and fabrication process of the self-propelled soft robot. All robot parts (except the miniature camera) were made by molding technique.

to be ten times that of an air chamber. In this configuration, the robot always has at least two contact points with its environment while being short enough not to obstruct movement at areas with bends.

B. Control and Locomotion Strategies

We define a segment as a unit comprising two opposing air chambers and the part of air path corresponding to them as an actuation unit. The robot is divided into five continuous segments, each comprising two nearby actuation units. To achieve smooth sinusoidal wave movement, each segment is able to deform into one of four modes including crest, trough, transient from crest to trough, and transient from trough to crest. Fig. 3(a) illustrates a cycle of bending for a segment. Pressurized air is supplied in order that the segments change status between four modes periodically, based on the working principle proposed in [18]. This results in propagation waves from end to end of the robot body, as shown in Fig. 3(b), which gives both forward and backward movement depending on the propagation wave direction.

In the scenario of vertical locomotion in a constrained environment such as a tube or colon, the robot achieves climbing motion through intermittent attachment and detachment along its environment at a number of points, called anchor points (yellow circles) and moving points (green circles), as in Fig. 3(c). To create anchor points, soft actuators are pressurized so inflated sections press against the wall, in effect the peaks of the sine wave are flattened because they are constricted by the environment. As described above, the balloon at the tail is inflated on one side only, which provides more contact area with the surrounding wall, preventing the robot from slipping down. Such activation reduces friction between the balloon and wall, which prevents vertical movement of the robot, compared to the use of a symmetrical balloon. This results in a difference in the height of the robot between different time steps.

To achieve undulatory locomotion, control signals for four solenoid valves that route pressurized air into four air channels operate as shown in Fig. 3(d). Compared to the strategy proposed in [18], we include a quarter-period shifting phase between each control signal, which ensures smoother transitions among the four bending modes. Regarding the operation of the robot, each air channel is connected to a 4/2-way solenoid valve with ports 1 to 4 (VQD 1121-5L; SMC, Japan). A similar unit is connected to the four chambers of the steering component. Air pressure to the system by the compressor (AC462XGB, Makita, Japan) is adjusted by throttle and regulator valves. Fig. 4 is a schematic of the system. A Sony Spresense board (Sony, Japan) microcontroller provides the controlling program to the solenoid valves in a multithreading manner, in which each air channel and the steering are assigned independent control threads.

IV. Robot's Modeling

In this section, we propose kinematic and force models for horizontal locomotion. A model for vertical locomotion is not presented in the current study since this scenario contains a complicated stick-slip phenomenon between the robot and its surroundings. The kinetic model is based on geometrical assumptions reported by Nguyen and Ho [6] plus factors representing conditions of terrestrial locomotion. The aim of this model is to predict the speed of the robot when moving at a constant velocity. For the force model, we exploit the elastic property of the inflated actuation units, therefore, the whole body of the robot can be considered as a system of compressed torsion springs. The results of the kinematic and force models could be useful for future modeling of locomotion in a variety of environments and in developing control strategies.

A. Kinematic Model for Horizontal Locomotion

Fig. 5 illustrates the dorsal view of the moving robot and the schematic of geometry and velocity. Two assumptions are adopted, which are: 1) The shape of the robot is considered as a

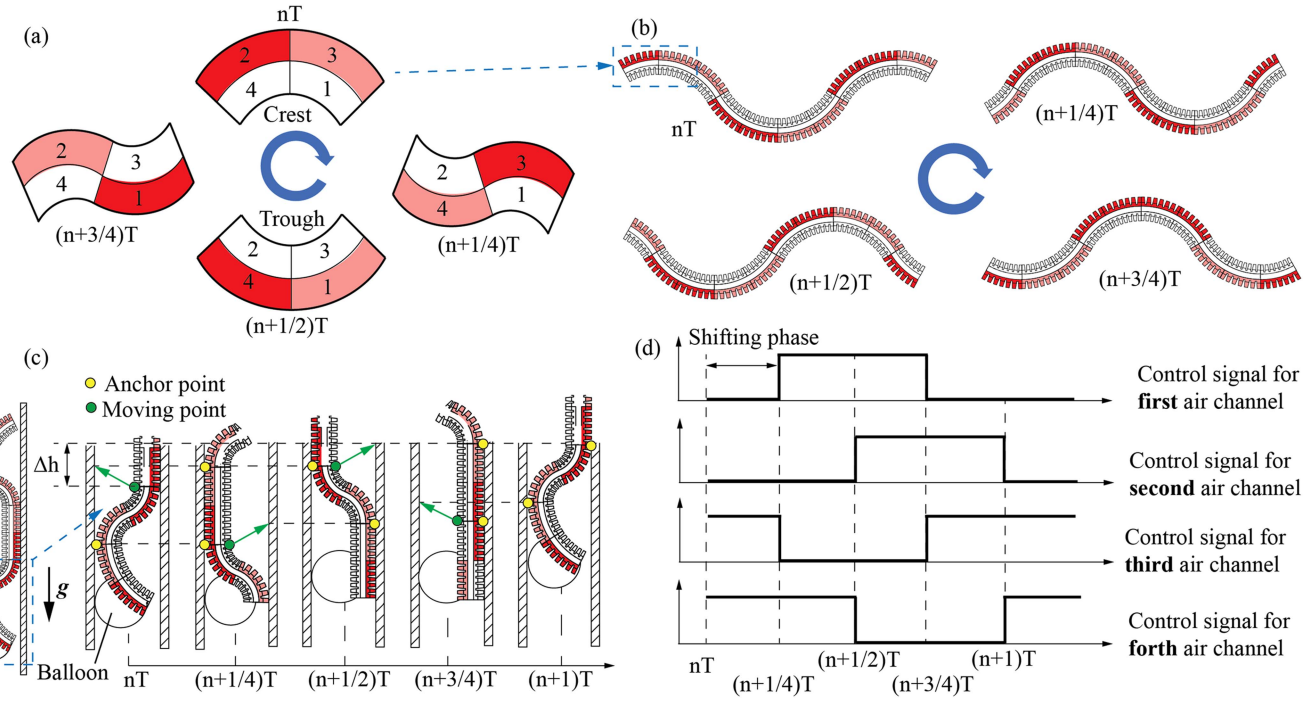

Fig. 3. Strategy for robot locomotion. (a) Bending modes of the first segment in one period based on study in [18]. (b) Posture of the robot body in one period during horizontal locomotion. (c) Posture of the robot tail in one period during vertical locomotion. (d) Pressure control signals for four air channels. T denotes time period. Red denotes air chamber inflated by pressurized air for T/2, pink denotes air chamber inflated by pressurized air for T/4.

sinusoidal wave with amplitude A, wavelength λ, and frequency f. 2) The robot is assumed to not slip against the environment when performing locomotion, in other words, friction between the robot body and its surroundings is static friction. We consider point A_0 which is the point on the midline of the robot with maximum lateral displacement. The following can be concluded:

$$\begin{cases} \sin\left(\frac{2\pi}{\lambda}x_0 - 2\pi f t\right) = 1 \\ \cos\left(\frac{2\pi}{\lambda}x_0 - 2\pi f t\right) = 0 \end{cases} \tag{1}$$

where x_0 is the position of point A_0 on the axis x. A_1 is the point on the right side of A_0. The distance between them is Δx, which is infinitesimal. The position of A_1 can be expressed as

$$y_1 = A\sin\left[\frac{2\pi}{\lambda}(x_0 + \Delta x) - 2\pi f t\right]. \tag{2}$$

The speed at point A_1 is calculated as

$$\begin{aligned} v_1^y &= -2A\pi f\cos\left[\frac{2\pi}{\lambda}(x_0+\Delta x) - 2\pi f t\right] \\ &= -2A\pi f\left[\cos\left(\frac{2\pi}{\lambda}x_0 - 2\pi f t\right)\cos\left(\frac{2\pi}{\lambda}\Delta x\right)\right] \\ &\quad + 2A\pi f\left[\sin\left(\frac{2\pi}{\lambda}x_0 - 2\pi f t\right)\sin\left(\frac{2\pi}{\lambda}\Delta x\right)\right]. \end{aligned} \tag{3}$$

By substituting (1) into (3), we get

$$v_1^y = 2A\pi f\sin\left(\frac{2\pi}{\lambda}\Delta x\right). \tag{4}$$

The angular speed with respect to the origin A_2, which is the point making contact with the environment and is static due to the assumption of nonslipping, is expressed as

$$\omega = \frac{v_1^y}{\Delta x} = \frac{2A\pi f\sin\left(\frac{2\pi}{\lambda}\Delta x\right)}{\Delta x} \tag{5}$$

Since we only consider the magnitude of the angular speed and Δx approaches zero

$$\omega = 4A\pi^2\frac{f}{\lambda}. \tag{6}$$

The speed of horizontal locomotion can then be calculated as the forward speed at point A_0

$$v_{\text{horizontal}} = v_0^x = \omega r = 4Ar\pi^2\frac{f}{\lambda} \tag{7}$$

where r is the radius of the robot body. The amplitude A depends on the nature of the robot's body and will be determined experimentally. The wavelength can be calculated by using the following method. Firstly, the distance with the length of $\lambda/4$ is divided into n equal parts. We then acquire n right triangles of which sides are colored in cyan, as shown in Fig. 5. For the ith triangle, the hypotenuse can be calculated as

$$\begin{aligned} l_i &= \sqrt{(x_i - x_{i-1})^2 + (y_i - y_{i-1})^2} \quad (i = 1, 2, .., n) \\ &= \sqrt{\frac{\lambda^2}{16n^2} + \left\{A\sin\left(\frac{i\pi}{2n}\right) - A\sin\left[\frac{(i-1)\pi}{2n}\right]\right\}^2} \\ &= \sqrt{\frac{\lambda^2}{16n^2} + \left(2A\cos\frac{\pi(2i-1)}{4n}\sin\frac{\pi}{4n}\right)^2}. \end{aligned}$$

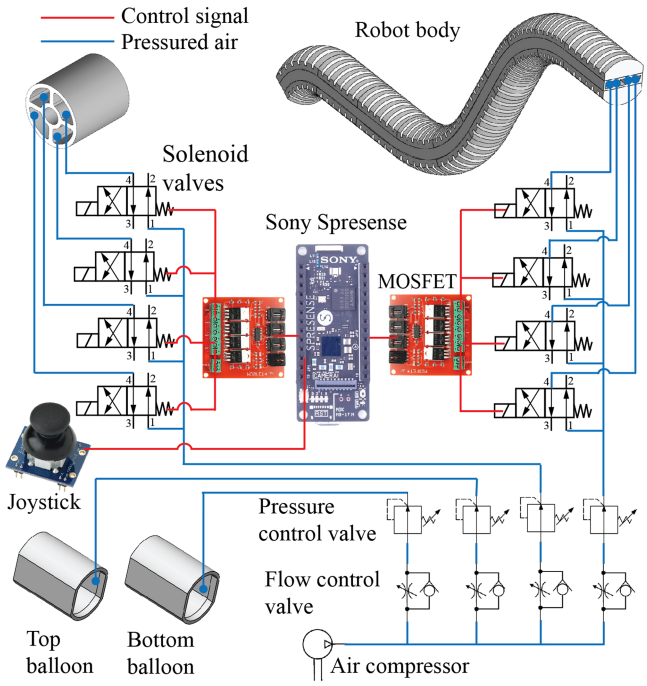

Fig. 4. Diagram of control system. Sony Presense and Mosfet circuits were used to control the on/off statuses of eight solenoid valves that contribute pressurized air to four air channels. Four mechanical flow and pressure control valves were used to adjust air pressure working on the robot.

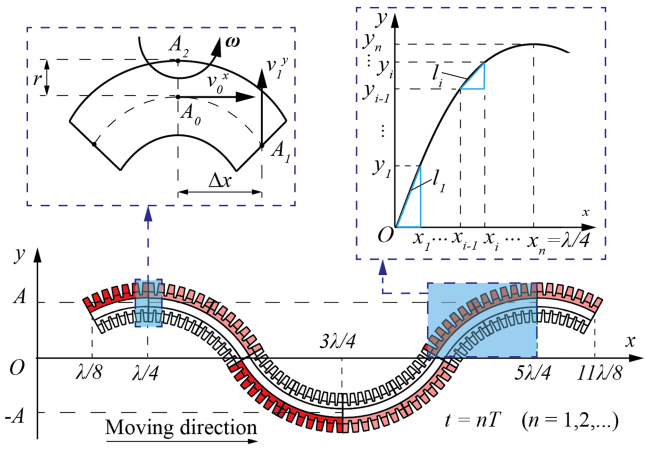

Fig. 5. Illustration of schematic for kinematic model for colonoscopy robot. The red and pink parts denote air chamber inflated by pressurized air. Different colors indicate the difference in inflation duration.

The sum of the length of all triangles gives us the length of a curve equal to two actuation units. Therefore, the wavelength can be calculated by solving the following equation:

$$\sum_{i=0}^{n}\sqrt{\frac{\lambda^2}{16n^2}+\left(2A\cos\frac{\pi\,(2i-1)}{4n}\sin\frac{\pi}{4n}\right)^2}-2L=0. \quad (8)$$

The wavelength acquired from (8) is substituted into (7) to calculate the velocity of the robot, which is then compared with the experimental results in Section VI.

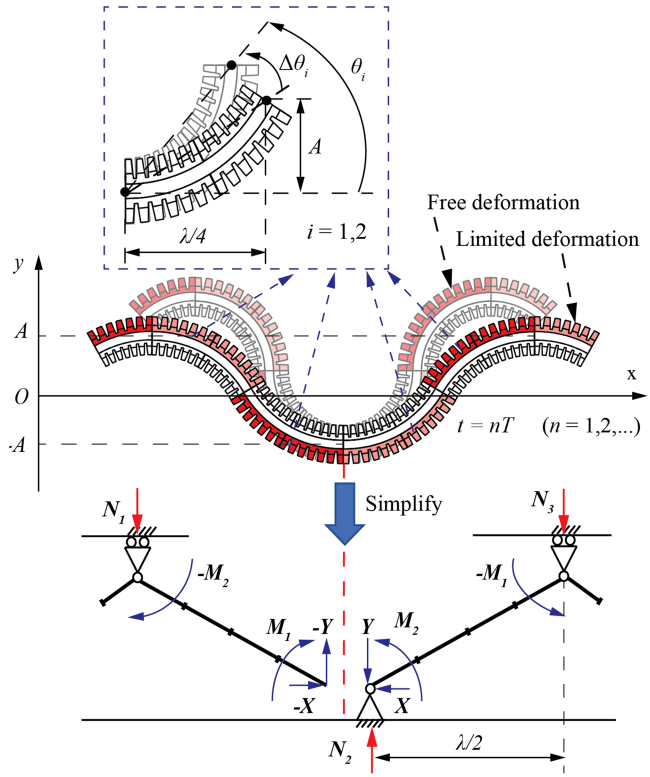

Fig. 6. Illustration of force model. The red and pink parts denote air chamber inflated by pressurized air. Different colors indicate different inflation durations.

B. Lateral Force Model for Horizontal Locomotion

When the robot body bends by inflation of the actuators, it is restricted by the confined workspace resulting in a counterforce against its environment. We assume that the lateral force is mainly caused by such counterforce. The reason is that the force caused by the lateral acceleration of the robot body is relatively small and can be negligible due to the light weight of the robot and little impact time. A pair of two inflated in-phase continuous actuation units is represented as a torsion spring. We consider the time step of $t = nT\ (n = 1, 2, \ldots)$, since at this posture, the robot is in most contact with the two sides of its surroundings, which results in a maximum force value. As seen in Fig. 6, due to the control strategy, the robot body is not inflated evenly, the red parts have been inflated for a period of $T/2$, while the period for the pink part is $T/4$. The blurred illustration demonstrates the shape of the robot if it were freely deformed. In the case of free deformation, the bending angle for the red part can be calculated as

$$\theta_1=\begin{cases}2\omega_{\text{be}}\frac{T}{2}=\frac{\omega_{\text{be}}}{f} & \text{if } \frac{\omega_{\text{be}}}{f}<\theta_{\max},\\ \theta_{\max} & \text{if } \frac{\omega_{\text{be}}}{f}\geq\theta_{\max}\end{cases} \quad (9)$$

and for the pink part is

$$\theta_2=\begin{cases}2\omega_{\text{be}}\frac{T}{4}=\frac{\omega_{\text{be}}}{2f} & \text{if } \frac{\omega_{\text{be}}}{f}<\theta_{\max}\\ \theta_{\max} & \text{if } \frac{\omega_{\text{be}}}{f}\geq\theta_{\max}\end{cases} \quad (10)$$

TABLE I
OPERATIONAL INPUTS AND MEASURED DATA FOR CALIBRATION AND VALIDATION EXPERIMENTS

	Calibration Experiment		Validation Experiment	
	A	B	C	D
Pressure (kPa)	65, 70, 75, 80, 85, 90, 95		70, 80, 90	65, 75, 85
Frequency (Hz)	None		1.0, 1.5, 2.0, 2.5, 3.0	1.0, 1.25, 1.5
Measured data	ω_{be}, θ_{max}	k	A, v, N	v, N

where ω_{be} and θ_{max} are the bending speed and maximum bending angle of one actuation unit, respectively. The limited deformation resulting from the presence of the tube causes a decrease in the bending angle of the torsion spring. This amount of decrease for the red and pink parts can be calculated as

$$\Delta\theta_i = \theta_i - \arctan\left(\frac{4A}{\lambda}\right) \quad (i = 1, 2) \tag{11}$$

where the wavelength λ is acquired from (8). The bending moment exerted by the deformed torsion spring is expressed as

$$M_i = \frac{k\Delta\theta_i}{2} \quad (i = 1, 2) \tag{12}$$

where k is the torsion spring constant of one actuation unit. The robot body is then expressed by a system of beams to realize the exerting force. The beam system is statically indeterminate and is solved by cutting the structure. The lateral forces acting on the robot body are calculated as

$$\begin{bmatrix} N_1 \\ N_2 \\ N_3 \end{bmatrix} = \begin{bmatrix} 1 & -1 & -1 \\ \lambda/2 & 0 & 0 \\ 0 & 0 & \lambda/2 \end{bmatrix}^{-1} \begin{bmatrix} 0 \\ M_1 + M_2 \\ M_1 + M_2 \end{bmatrix}. \tag{13}$$

The parameters ω_{be}, θ_{max}, and k will be obtained through experiments. Using (13) we can calculate the lateral force caused by the robot and the results are subsequently compared with values obtained in experiments, which is presented in Section VI.

V. MEASUREMENT OF ROBOT'S CHARACTERISTICS

In this section, two groups of experiments are conducted to 1) realize the parameters needed to complete the kinematic and force models proposed in Section IV (Calibration experiments); 2) examine the effects of the input parameters on velocity and lateral force, and compare the results with the model prediction (Validation experiments). Horizontal and vertical locomotion are considered. The experiment apparatus included: a power supply (U8001A, Keysight, USA); high-speed camera (DSC-RX10M4; Sony, Japan); digital force gauges (ZTS-5N, IMADA, Japan); pressure sensor (ISE30A-C6H-N-M, SMC, Japan); flow rate sensor (PFM710-01-A, SMC, Japan); an acrylic tube 500 mm long with a 45 mm inside diameter. Each experiment was repeated three times with the results averaged. For extracting and processing the experiment data, the selected software was MATLAB R2021b (MathWorks). Table I summarizes the operational inputs and measured data of the experiments.

A. Calibration Experiments

In the case of the lateral force model, the needed properties are the angular bending speed ω_{be}, maximum bending angle θ_{max}, and torsion spring constant k. For the kinematic model, the unspecified parameter that can be experimentally acquired is the amplitude A. The following experiments aim to realize the mentioned parameters, except for amplitude A, which is addressed in the subsequent section.

1) Experiment A—Measuring of Angular Bending Speed and Maximum Bending Angle of One Actuation Unit: In this experiment, a single actuation unit was fixed at one end and inflated to its maximum bending by pressurized air at 65, 70, 75, 80, 85, 90, or 95 kPa. Below this pressure range, the actuation unit revealed low bending efficiency, meanwhile beyond it deformed excessively and was close to failure. The high-speed camera was placed 300 mm above, as shown in Fig. 7(a), and recorded the deformation progress. The footage was cut into frames using MATLAB. The maximum bending angle was measured manually in the extracted image using a reference angle ruler with a resolution of one degree added to the image. By examining the recorded video, the bending time was deduced and the bending speed was calculated.

2) Experiment B—Identifying of Torsion Spring Constant: For this measurement, the single actuation unit was subjected to the same conditions as in Experiment A. A ZTS-5N force gauge was placed on a railway and pushed into the free end of the unit as in Fig. 7(b). The recorded force value was multiplied by the distance from the tip of the force gauge to the fixed end of the unit to calculate the corresponding bending moment value. The bending angles before and after the unit was pushed were similarly measured in Experiment A. The torsion spring constant was deduced from the difference in bending angle (between before and after the unit was pushed by the force gauge) and the resulting bending moment.

B. Validation Experiments

In this section, experiments were conducted to obtain the velocity and lateral force during robot locomotion.

1) Experiment C—Measuring of Velocity, Lateral Force, and Amplitude of Horizontal Locomotion in Acrylic Tube: The experiment was performed with the chosen sets of system pressures and frequencies of (70, 80, 90 kPa) and (1.0, 1.5, 2.0, 2.5, 3.0 Hz), respectively. The robot was moving inside an acrylic tube 500 mm long and 45 mm. A high-speed camera situated 500 mm above the tube recorded the movement of the robot, and images were extracted from the footage using MATLAB to realize the traveling time of the robot. To measure lateral force, the acrylic tube was cut in half, and a 30 mm long acrylic

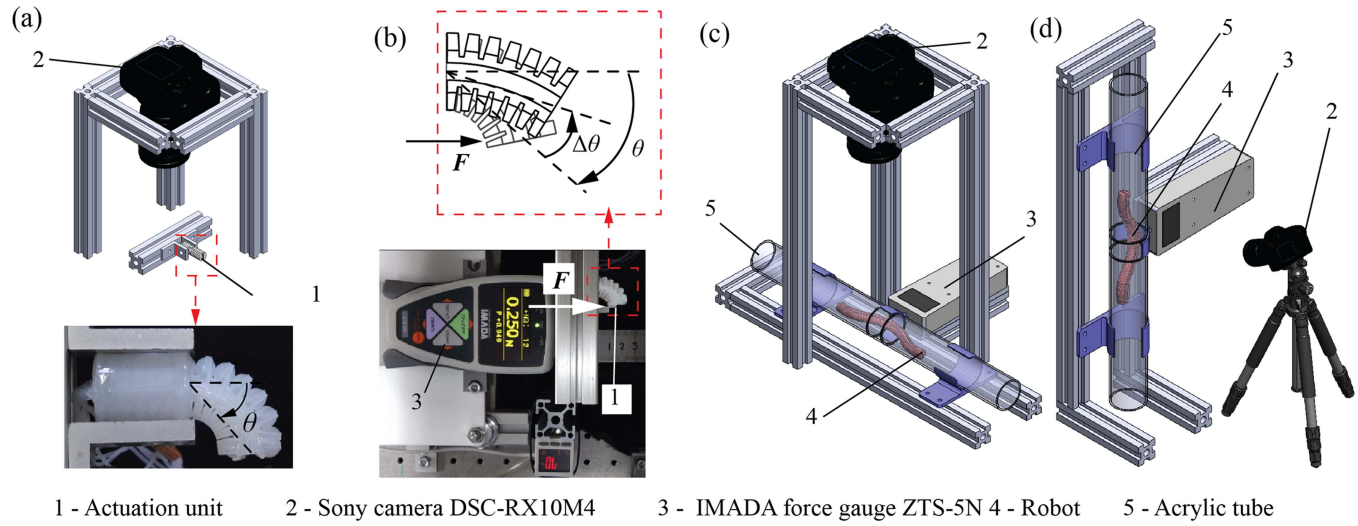

Fig. 7. Experimental setups. (a) Maximum bending angle and bending speed measurement experiment. (b) Experiment to determine torsion spring constant. (c) Horizontal velocity and lateral force in acrylic tube measurement experiment. (d) Vertical velocity and lateral force in acrylic tube measurement experiment.

ring connected to a ZTS-5N force gauge was placed between the two halves of the long tube, as in Fig. 7(c). The value of force at the moment the middle of the robot made contact with the ring, which corresponded to the considered posture of the force model in Section III was recorded. Finally, the value of the robot amplitude was measured by adding a reference ruler with a resolution of 0.5 mm into the extracted images.

2) Experiment D—Measuring of Velocity and Lateral Force of Vertical Locomotion in Acrylic Tube: In this experiment, the setup in Experiment C was placed vertically as in Fig. 7(d). The set of input parameters included pressure of (65, 75, 85 kPa) and frequency of (0.75, 1.0, 1.25, 1.5, 1.75 Hz). In addition, the effect of the balloon at the tail of the robot at three inflation pressures, 0 (inactivation), 10, and 20 kPa was examined. The robot performed upward vertical self-propulsion with the support of a balloon and the data collecting and processing for velocity and force was conducted similarly to Experiment C.

VI. Results

A. Locomotion Capability Modeling and Horizontal Locomotion

Fig. 8(a) shows the advanced movement of the robot in one cycle, which accords to the horizontal locomotion strategy proposed in Section III-B. To realize the kinematic model in Section IV-A, the amplitude of the sine wave was first determined. We considered the variation amplitude to be a function of input pressure P and frequency f. The function is realized by using the curve fitting tool of MATLAB and utilizing the Trust-Region method on the data set of 15 data points of amplitude collected from Experiment C, which is presented in Table II. The function $A(P, f)$ is described in Table IV with an R-squared value of 0.970. With the establishment of a function for amplitude, from a set of pressure P and frequency f, the horizontal velocity could be subsequently calculated using (8) and (7) from the input parameters in Experiment C and

TABLE II
Results for the Measuring of Amplitude

P (kPa) \ f (Hz)	1.0	1.5	2.0	2.5	3.0
70	10.5 mm	10 mm	6 mm	5.5 mm	4.5 mm
80	12 mm	11.5 mm	7 mm	7.5 mm	6 mm
90	13 mm	12 mm	10 mm	9 mm	7 mm

examined alongside the experimental results, as shown in Fig. 8(b). Both experimental and modeling results show velocity increased with pressure, this was also true in the rubber colon environment. Regarding the relationship between horizontal speed and frequency in the acrylic tube, as frequency increased, velocity reached a peak before starting to decrease. Predictions from the kinematic model revealed a similar tendency with a slight deviation. The highest recorded velocity for the rigid environment was 40.11 mm/s, corresponding to 0.171 Body-Length/s (BL/s), achieved at 90 kPa of pressure and 2.5 Hz of frequency. This is considerably faster than the performance reported by Lin et al. (27 mm/s–0.176 BL/s) [15], Manfreidi et al. (2.8 mm/s–0.047 BL/s) [16], and Qi et al. (35 mm/s) [18].

The difference between the model and experimental values is quantified through percentage error, computed as follows:

$$\text{Error} = \frac{|V_{\text{experiment}} - V_{\text{model}}|}{V_{\text{experiment}}} \tag{14}$$

where $V_{\text{experiment}}$ is the data acquired from experiments and V_{model} is estimated by the models. The percent error for the velocity prediction is 7.89%.

B. Interaction Forces Modeling

There are several factors contributing to an incomplete colonoscopy process, including patient discomfort and pain. The capability of colonoscopy has been enhanced by the use of soft robotics solutions. Nevertheless, excessive colon deformation and/or interaction forces can still cause discomfort due

TABLE III
RESULTS FOR THE MEASURING AND IDENTIFYING OF BENDING SPEED, MAXIMUM BENDING ANGLE, AND TORSION SPRING CONSTANT

P (kPa)	65	70	75	80	85	90	95
ω_{be} (s^{-1})	1.27	1.51	1.64	1.64	2.09	2.16	2.39
θ_{max} (rad)	0.785	0.785	0.960	1.05	1.05	1.22	1.31
k (N m rad^{-1})	16.1	16.9	22.7	22.9	26.1	26.2	30.5

TABLE IV
COEFFICIENTS AND R-SQUARE OF FUNCTIONS FORMED OF: $g(P,f) = p_1 + p_2P + p_3f + p_4P^2 + p_5Pf + p_6f^2$ FOR AMPLITUDE, BENDING SPEED, MAXIMUM BENDING ANGLE AND TORSION SPRING CONSTANT

	p_1	p_2	p_3	p_4	p_5	p_6	R-squared
A (mm)	-20.4	0.0875	15.8	0.00167	-0.0750	-2.33	0.970
ω_{be} (s^{-1})	-1.12	0.0367	0	0	0	0	0.956
θ_{max} (rad)	-0.424	0.0181	0	0	0	0	0.956
k (N m rad^{-1})	-14.1	0.465	0	0	0	0	0.944

to colonoscope movement. To ensure that the robot has potential application in the endoscope, prediction, and evaluation of interaction forces should be considered in the development process of colonoscopy robots. To complete the force model proposed in Section IV-B, we first established the expressions of bending speed, maximum bending angle and torsion spring constant as functions of pressure P. We also used the curve fitting tool of MATLAB on the data points reported in Table III to derive the functions $\omega_{be}(P)$, $\theta_{max}(P)$, and $k(P)$, which are shown in Table IV, where the R-squared values are 0.956, 0.956, and 0.944, respectively. The mentioned data were obtained from Experiments A and B. Similar to the horizontal velocity, lateral force in horizontal locomotion could be calculated from the input pressure and frequency using (13). The force model was applied to simulate the maximum lateral force that the robot exerted onto the sides of its constrained environment. The experimental and simulated results are presented in Fig. 8(c). It is clear that lateral force increased corresponding to a rise in pressure, this was true for both the experiment and model. The simulation also agreed with the experimental data regarding decreased lateral force with frequency increase. The highest value of lateral force recorded was 0.63 N and the lowest was 0.14 N, which were achieved at pressures and frequencies of (90 kPa, 1.0 Hz) and (70 kPa, 3.0 Hz), respectively. The percent error for the interaction force estimation is 16.86%.

C. Vertical Locomotion With Support of Balloon

In the case of vertical locomotion, it was found that the robot could only operate reliably at a narrower range of input parameters compared to horizontal locomotion. To be specific, for the scenario of climbing in the acrylic tube, the necessary pressure was 75 kPa, frequency was within the set of (1.0, 1.25, 1.5 Hz), and the balloon activated at 10 kPa.

The results of Experiment D, shown in Fig. 9(a), support the vertical locomotion strategy proposed in Section III-B. The one-end inflated balloon successfully prevented the robot from slipping while still allowing for sinusoidal wave movement. Fig. 9(b) illustrates the experimental results of velocity and lateral force in robot vertical locomotion. Velocity in the acrylic tube increased with frequency and peaked at 9.22 mm/s (0.039 BL/s), achieved at 1.5 Hz of frequency. In contrast with velocity, lateral force in vertical motion slightly decreased as frequency increased, showing the highest force of 0.33 N recorded at 1.0 Hz, and the lowest force of 0.31 N recorded at 1.5 Hz.

Fig. 9(c) shows the use of the head balloon and the steering mechanism. The robot traveled to a decided position and the head balloon was inflated. The robot anchored itself while the handheld joystick was used to adjust the camera angle, providing a clear vision of a marker placed on the inside of the acrylic tube.

D. Cost of Transport

The effectiveness of robot locomotion can be evaluated through the cost of transport (COT), which represents the amount of energy needed for the travel. For the proposed inspection robot, the consumption energy comes from two sources, namely electrical power to operate the control system and air pressure power to inflate the robot components. Therefore, COT can be defined as

$$\text{COT} = \frac{(UI + PQ)\,t}{mgd} \tag{15}$$

where U is supply voltage, I is current, Q is flow rate, m is mass of the robot, g is gravitational acceleration, and d is travel distance. The voltage and current were measured by sensors integrated into the power supply while the pressure and flow rate were read from the pressure and flow rate sensors. Fig. 10 shows the results for the calculation of COT for the different cases of locomotion. The COT values were high due to the robot's small size, even though our maximum input pressure was relatively low at 90 kPa compared to the 172 kPa used in [18]. The data of COT were in good agreement with the previous results on velocity, to be more specific, lower COT correlates with faster movement. The minimum value of COT was 4.5773×10^3 corresponding to the maximum speed of 40.11 mm/s, which was achieved at the pressure of 90 kPa and frequency of 2.5 Hz. The examination of COT is valuable in selecting the most suitable input parameters for each operating scenario.

VII. WORKING OF ROBOT IN COMPLEX ENVIRONMENT

To evaluate the robot's potential for inspection tasks, we tested its capabilities in complex terrains composed of various materials. Two representative groups of materials, deformable and nondeformable terrains, were selected to simulate different interaction scenarios. The robot's locomotion is significantly

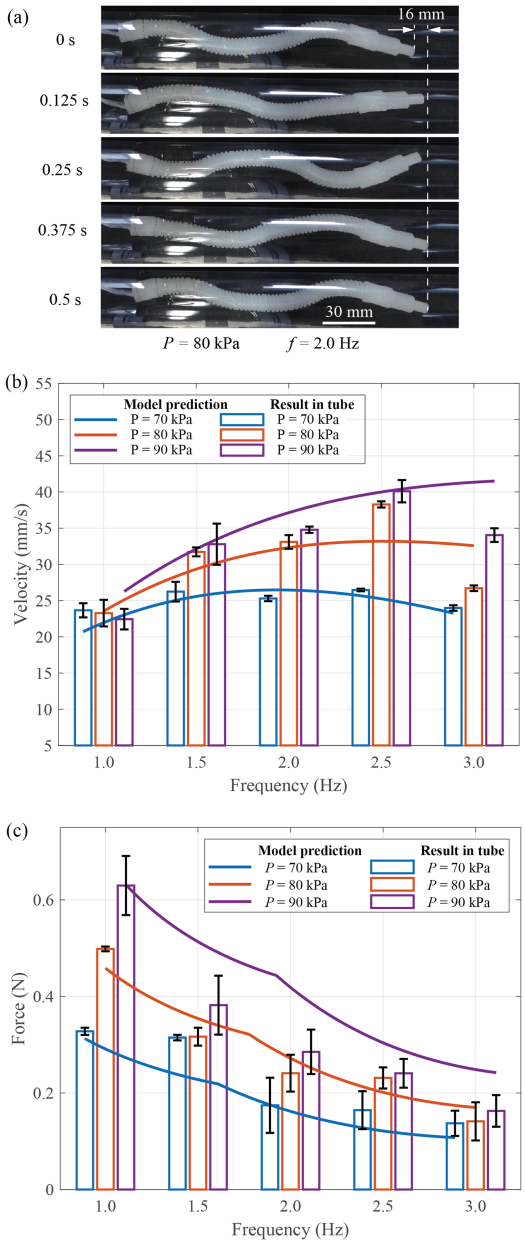

Fig. 8. Results for horizontal locomotion experiments. (a) Wave-like motion of the robot in one period. (b) Comparison of horizontal velocity at different input pressures and frequencies. (c) Comparison of horizontal lateral force at different input pressures and frequencies.

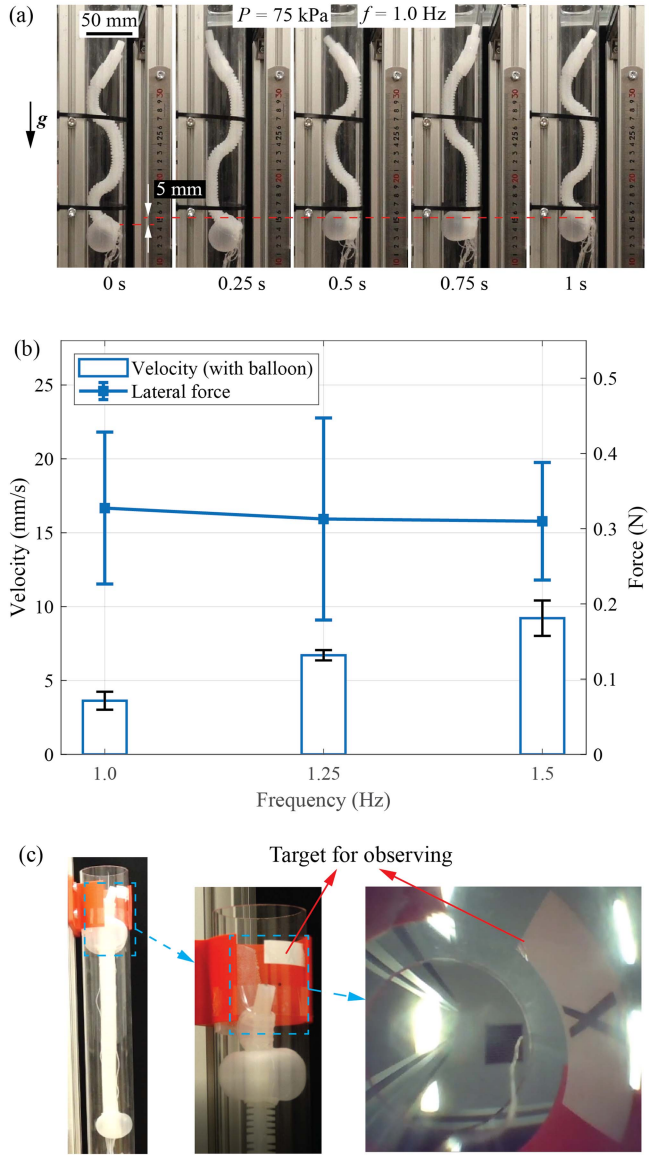

Fig. 9. Results for vertical locomotion experiments. (a) Posture of the robot in one period. (b) Comparison of vertical velocity and lateral force at different input pressures and frequencies. (c) Anchoring in a vertical tube by inflating the head balloon and observing a target.

influenced by the deformation of tube walls and the friction coefficient between the tube walls and the robot body. In this study, the deformability and shape of the intestinal wall were simulated using phantom colon environments. The phantom colon is utilized because the colon has challenging locomotive conditions, including a soft wall, fewer constraints, and complex shapes, which aids in evaluating the robot's performance.

A. *Locomotion in Rigid Tube Systems*

This section examines the operation of the robot in systems of rigid tubes.

1) Horizontal U-Shape Acrylic Tube System: In this test, a series of acrylic tubes were connected and laid out horizontally to form a U-shape tunnel, the dimensions are given in Fig. 11(a). The robot operated under inputs of (80 kPa, 2.0 Hz) and (80 kPa, 2.5 Hz). It successfully went through 90° turns and the times taken to complete the 86 cm horizontal U-shape route under frequencies of 2.0 Hz and 2.5 Hz were 93 s and 52 s, respectively.

2) U-Shape Acrylic Tube System With Vertical Section: The setup for this test is shown in Fig. 11(b). In this task, the robot failed to reliably go through a 90° turn, since it had no effective strategy to change direction. An elbow connector with a 45° slope was placed between two tubes to enable replication of navigation through the turn section. After the robot had gone through the first turn and was positioned vertically, the bottom balloon

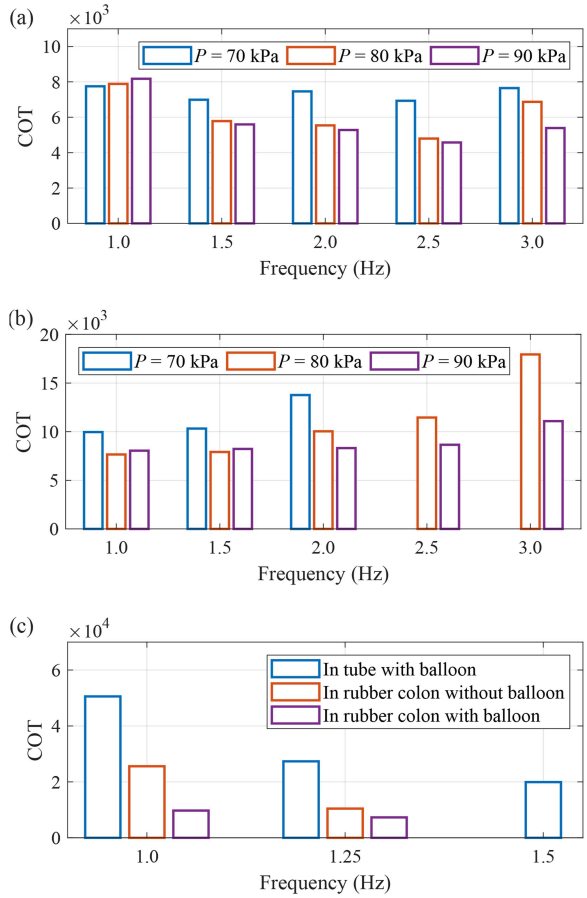

Fig. 10. Comparison of COT at different input values of pressure and frequency. (a) Horizontal locomotion in tube. (b) Horizontal locomotion in rubber colon. (c) Vertical locomotion.

was inflated to support climbing. The balloon was then deflated after the robot had gone through the second elbow connector and returned to the horizontal locomotion phase. The chosen value for pressure was between 75 and 80 kPa (the pressure was changed slightly as the robot moved in different sections). The frequency was set to 1.0 Hz because it was found that the experiment was most stable and replicable at this condition. The robot took 3 min 20 s to complete the U-shape route including horizontal and vertical sections amounting to a total length of 83 cm.

3) Locomotion in Tube Containing Lubricants: In this section, we conducted tests on the robot in environments that were lubricated with liquid substances. As depicted in Fig. 11(c), the robot navigated through a straight acrylic tube with the inner surface coated with cooking oil. The experiments were carried out at working pressures of 70, 80, and 90 kPa, while the frequency ranged between 2.0 and 2.5 Hz. The results were then compared with the performance in dry tube. There is a noticeable decrease in velocity when oil is included in the environment, as seen in Fig. 11(c). Specifically, in the liquid-included tube, the robot achieved a maximum speed of 27.97 mm/s, whereas in the dry tube, the speed reached 40.11 mm/s. This decrease in velocity can be attributed to the reduced friction force, which is a crucial factor for the robot's locomotion, as explained in Section IV. It should be noted that, due to insufficient friction, the robot's current design and control strategies do not enable it to vertically climb in an oil-coated tube.

B. Locomotion in Phantom Colons

We investigate the effectiveness of our robot in phantom colon arrangements with different levels of complexity, constraint and softness. Two colon phantoms were used as the test environments: the first is a rubber colon tube from Kyoto Kagaku Company, Ltd. (referred to as the KK phantom colon), and the second is an Ecoflex phantom colon that we fabricated. Table V summarizes the conditions and results of the tests. The input parameters were set at 80–85 kPa pressure and 1.0 Hz frequency.

1) Straight Section of KK Phantom Colon: We conducted a stress-strain test which indicated that the rubber colon had a Young's Modulus of 0.34 MPa. This shows that the phantom model has a similarly low stiffness compared to a human colon which has a Young's Modulus as low as 0.63 MPa [43]. A phantom segment 500 mm in length was placed on a flat surface and secured using plastic braces with one end opened for the colonoscopy robot to enter, and the other end connected to a ZTS-50N digital force gauge. Fig. 12(a) shows the setup and result of this test. The input pressure and frequency were the same as in Experiment C. The robot performed self-propelling inside the rubber colon until its arrival at the other end of the colon was detected by the digital force gauge and traveling time was recorded. The results of locomotion in the rubber colon shows a different trend compared to the locomotion in rigid tube. The value of velocity gradually decreased with increasing frequency. The robot showed no forward movement at a low pressure of 70 kPa and high frequency of 2.5 and 3.0 Hz while it best performed at 80 kPa of pressure and 1.5 Hz of frequency, reaching a maximum speed of 23.20 mm/s (0.099 BL/s).

The phantom colon section was then set upright. Fig. 12(b) shows the setup and result of this test. When moving in this configuration, the robot required the input pressure of 75 kPa while the choices for frequency were limited to 1.0 or 1.25 Hz. Interestingly, the robot could scale the rubber colon with or without the support of the bottom balloon. With the support from a balloon of 10 kPa air pressure, velocity greatly improved, and the robot moved the fastest at 25.16 mm/s (0.107 BL/s), achieved at a frequency of 1.25 Hz.

2) Tube-Constrained KK Phantom Colon With Vertical Sections: The KK phantom colon was placed in a system of connected tubes to simulate the shape of the human colon, as shown in Fig. 12(c). Air was pumped into the colon to ensure the elastic wall did not collapse onto the robot. The robot was able to complete locomotion through the 1.5 m long rubber colon in 3 min 14 s, which means the average velocity was 6.96 mm/s (0.030 BL/s). To perform the return journey, the order of the air channel inflation was reversed, which resulted in a backward propagation wave and backward motion. Pulling support was assisted by a human and the retrieval of the robot took 1 min 10 s. To mitigate the challenge of lateral swinging in the camera view during wave-like locomotion, we have developed a Python

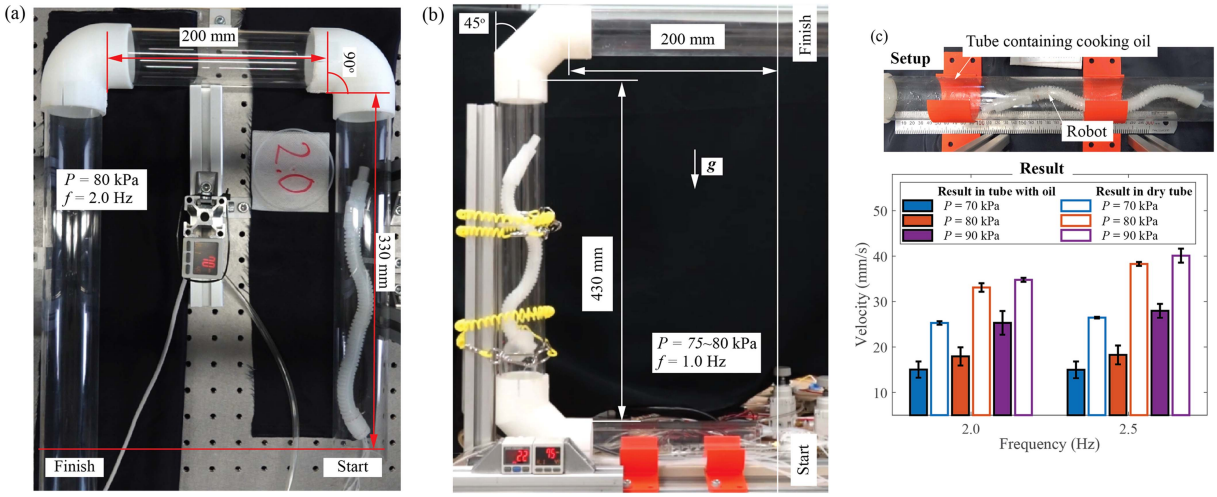

Fig. 11. Locomotion of the robot in U-shape rigid tube systems. (a) Setup and performance of the robot in horizontal tubes (on a table, the gravity does not resist the robot). (b) Setup and performance of the robot when moving from horizontal to vertical tube. (c) Setup and result for test of robot traversing tube coated with cooking oil.

TABLE V
SUMMARY OF THE TEST SETUPS AND RESULTS IN PHANTOM COLONS

	Straight Kyoto Kagaku Phantom Section		Kyoto Kagaku Phantom Colon		Ecoflex Straight Colon-Like Tube	Ecoflex Phantom Colon
Orientation	Horizontal	Vertical	Horizontal and Vertical	Horizontal	Horizontal	Horizontal
Length (cm)	50	50	150	150	62.58	130
Constrained by	Thin Braces	Thin Braces	Tube	Cables	None	None
Lubrication	No	No	No	Yes	No	Yes
Air Inflating	No	No	Yes	No	No	Yes
Robot Completes the Route	**Yes**	**Yes**	**Yes**	**Yes**	**Yes**	**No**
Average Velocity (mm/s)	23.20 (max)	25.16 (max)	6.96	17.94	5.86	N/A

program that performs frame rate downsampling. Specifically, only the frames corresponding to the instances when the robot's head is oriented forward are retained. The program was subsequently applied to the footage captured inside the rubber colon, resulting in the provision of two windows on the monitor for the inspector's benefit. One window displays the original frame rate footage, while the other showcases the downsampled frame rate footage, which serves as a supportive visual aid and offers the inspector a more stable view. This setup is depicted in Fig. 12(e).

3) Loosely Constrained KK Phantom Colon: We then reduced the amount of constraint enforced on the phantom colon by replacing the tubes with four plastic cables, as seen in Fig. 12(d). The robot completed the route with an average velocity of 17.94 mm/s (0.076 BL/s).

4) Ecoflex Straight Colon-Like Tube: We fabricated a soft tube, which is shown in Fig. 12(f), based on the design of the phantom colon from [44]. Ecoflex 00-20 was chosen for its high biomechanical similarity, as it can effectively mimic the large deformation characteristics of a colon. The robot's average velocity in this scenario was 5.86 mm/s. Due to the low constraint enforced by the soft tube, the velocity greatly decreased compared to the results from Section VI.

5) Ecoflex Phantom Colon: A full-length 130 cm-long phantom colon, whose design and setup were based on the work from [44], was fabricated using Ecoflex 00-20, as seen in Fig. 12(g). This colon simulator was not constrained and although lubrication and inflating air were applied, the robot could NOT complete the route. The reason was that this version of the phantom colon was excessively soft, resulting in insufficient constraint for wave-like locomotion, and the robot could not pass through the bending sections.

VIII. DISCUSSION

A. Design and Fabrication

The casting method effectively enables the fabrication of a small, self-propelled robot with intricate internal cavities. The robot exhibits smooth locomotion waves suitable for traversing constrained environments. Its compact diameter of 16 mm, coupled with the ability to generate forward and backward propagation waves along its body, allows the robot to navigate narrow entrances and operate flexibly within confined spaces. Besides being able to move in horizontal space, the robot structure creates enough support points against the wall of its environment a suitable pressure to move vertically. A robot with a longer body (i.e., comprising a longer actuation unit or higher number of actuation units) may create more support points or a larger contact area with its environment. Such architecture might better keep the robot from sliding down, but it creates more friction hampering forward motion. This phenomenon has been proven experimentally in comparisons among shorter and

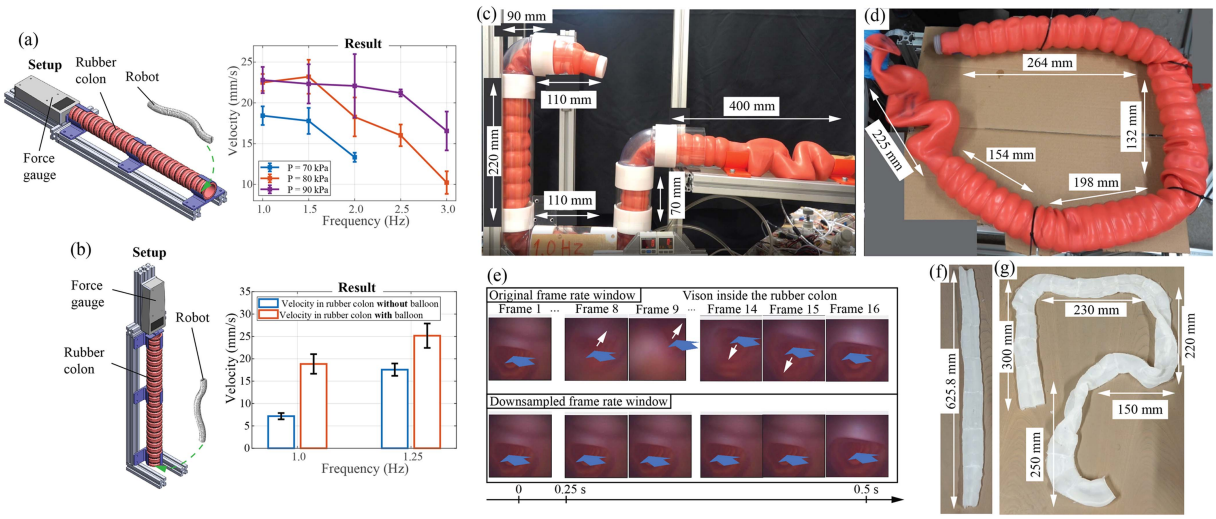

Fig. 12. Locomotion of the robot in soft environments. A section of the Kyoto Kagaku Phantom Colon is arranged horizontally (a) and vertically (b). The full-length Kyoto Kagaku Phantom Colon is tube-constrained (c) and loosely-constrained (d). We performed downsampling on the recording of vision inside the colon, the white arrow indicates the direction opposite to the swinging direction of the camera. We fabricated a colon-like tube (f) and a phantom colon (g) from Ecoflex 00-20.

longer robot bodies. However, the establishment of a theoretical, as well as simulation basis to optimize the length of the robot for best motion efficiency, is out of the scope of this study. Thus, experiments with different robot body lengths are not presented.

One drawback of the current design is that multiple distant air chambers are inflated by shared air channels, limiting the robot to a single type of locomotion—a sinusoidal wave. This means its movement direction is entirely dependent on the shape of the environment. Therefore, we aim to explore other configurations of air channels to control each part of the robot independently, expanding the range of environments and scenarios in which the robot can operate, such as a sigmoid colon. To support this update, future versions will investigate new positions, sizes, and shapes of the balloons.

Another important integration for achieving a fully functional inspection robot is the inclusion of localization mechanisms. In our current design, the mini camera enables vision-based estimation or segmentation [45], [46], while the balloons are suitable for tactile sensing techniques [47]. Future developments will further explore these perceptive Applications.

B. Control and Locomotion Strategies

The current locomotion strategies effectively work for routes that are straight or have curved sections of 90° or more, as evaluated in Section VI. With the addition of the tail balloon, our robot could navigate the elbow between horizontal and vertical sections and subsequently climb upwards of a U-shape tube system. Interestingly, the concept of asymmetrical inflation of the mentioned balloon also worked as intended, which prevented the robot from slipping down while allowing for wave-like locomotion. Aside from the rigid tube, the robot could also traverse the Kyoto Kagaku phantom colon, provided that the layout is kept simple and free of sharp curves.

However, when the surrounding walls were extremely soft, such as the Ecoflex phantom, the robot did not have sufficient constrain for the wave-live locomotion and failed to pass through the curved sections.

In the future, along with improvements in robot design, we aim to develop a locomotion pattern that is dedicated to routes with extreme curves and turns. Afterward, we plan to incorporate the vision information from the mini camera into the control of the robot.

C. Modeling

The proposed model for predicting velocity and lateral force for the case of horizontal locomotion successfully described the tendency of the examined properties. Nonetheless, a noticeable deviation between the model predictions and experimental results can be observed. The general reason was that the interaction between the robot body and its environment was highly complicated. The foremost problem was representing friction in the mathematical model. In our case, the contact points between the robot body and its surroundings and the magnitude of normal force at contact points altered throughout the locomotion of the robot. When traveling in an elastic environment such as the human colon, these factors become significantly harder to predict. A model for the vertical scenario was not presented in this article, as we believe that further study has to be conducted to elucidate the effect of gravity on the wave-like posture of a vertically ascending robot as well as the stick-slip motion. After clarifying the above factors, we would aim to develop a dynamic model for the self-propelled robot working in a variety of constrained environments The camera incorporated into the robot's body possesses a cable with a diameter of 0.66, which has no rigid outer layer. As a result, its inclusion did not produce a noticeable impact on the robot's performance, affirming the continued validity of the analytical models presented in this

article. Details on the examination of effect of cable stiffness on the results of velocity and lateral force are included in Appendix.

D. Locomotion Efficiency

The experimental results in Section VI have proven the ability of the proposed self-propelled robot to travel inside cylinder-shaped objects. We enhanced the locomotion strategy from [18] by adding shifting phases to improve horizontal movement and incorporating balloons to enable vertical navigation. When considering the scenario of horizontal locomotion, the three main factors that contributed to the performance of the robot are working pressure, frequency, and environmental specifications. The variation of the robot velocity in Fig. 8(b) indicated that working pressure strongly affects robot locomotion capability. The reason is that higher pressure creates greater lateral displacement, which geometrically improves the velocity. This correlation can be seen in (7). Better traction can also be achieved with higher pressure, as shown by the increase of lateral force in Fig. 8(c). Compared to pressure, frequency has a more nonlinear relationship with the velocity when the robot is moving in the acrylic tube, which can be explained as follows. At lower frequencies, the air chambers are inflated for a longer period of time resulting in a larger amplitude, which is geometrically favorable for the velocity. However, this also means slower undulation movement of the robot body. Therefore, there is an adversarial relationship between the two mentioned factors, which results in the velocity increases then decreasing as shown in Fig. 8(b).

Nonetheless, when the environment is changed to the rubber colon, increasing frequency only results in a decrease in velocity. The phenomenon is because the elastic phantom colon does not provide enough restraint, therefore, the lateral force that the robot exerts on the surroundings is greatly reduced at a higher frequency. This leads to insufficient friction and the robot cannot constantly remain in contact with the colon wall.

The robot also showed the ability to overcome terrain other than a straight and smooth route, which can be seen in the demonstration with the connecting section between a horizontal and vertical tube. Owing to its soft nature, when the robot hits the wall of the standing tube, its posture adapts to the curved course and then proceeds to climb upward.

In the case of vertical locomotion, frequency, environment, and the support of the balloon are the main factors that determine the performance of the robot. Similar to horizontal movement, velocity also has a nonlinear relationship with frequency as it rises to a peak and decreases to zero (the robot not moving). This comes from the phenomenon of slipping down of the robot. Specifically, during the process of vertically ascending, there are periods when the robot slips down, which is between the bending modes shown in Fig. 3(a). At a higher frequency, meaning the inflation period is shortened, the amplitude of the robot is not large enough to create sufficient friction to overcome slipping. Change of surrounding from a rigid tube to rubber colon resulted in an increase in velocity, which is opposite to the finding in the last scenario, and the robot could climb without using the balloon. The robot body could use the peak of the sinusoidal wave to "grab" onto ridges between segments of the colon, which reduces the slipping period. With the support of the balloon, this effect becomes even more relevant.

Researchers have determined that one of the reasons for incomplete endoscope procedures is pain caused by excessive colon stretching due to inflation and/or large interaction forces between instrument and colon wall. Due to the fact that force gauges cannot be installed inside the colon for the actual endoscope, it was necessary to use a hand grip that contained strain gauges around the endoscope's insertion tube in order to measure the clinician's forces on the endoscope during colonoscopy. Majority of this force can be attributed to the force acting on the colon wall (excluding the force of anal insertion). It was estimated that the interaction force was around 26 N, with anal insertion force at 18 N and peak pushing force at 44 N [48]. Also, Johnson et al. [49] reported that a force of 46.5 N is required to operate the colonoscopy process. Alternatively, some researchers have used a force sensor placed on the endoscope [50] or an arranged colon model [51] to evaluate the forces of interaction. For these two cases, the maximum force was approximately 13 and 4 N, respectively. Meanwhile, in our investigation, the maximum exerted force was just over 0.6 N. At best locomotion speeds, however, the robot's interaction force with the tube wall is only 0.3 N both horizontally and vertically. Interaction force values have been reported as being much smaller than in previous reports.

In short, the robot has shown the ability to traverse rigid tubular environments in various configurations while maintaining small interaction forces with the surrounding wall. Furthermore, the tests indicated the robot's potential to navigate soft environments, given sufficient structural support. If the wall is very soft, it meets significant challenges to move forward. This issue needs to be addressed in future work, in order to utilize this design for endoscope applications.

E. Contribution to Future Self-Propelled Robotic Colonoscopy

We compare some features in colonoscopy robots presented in literature, as shown in Table VI. Notably, the designs presented in [17], [27], [30], [52] were not evaluated for incline locomotion. Similarly, the works described in [26], [28], [29] propose techniques that can only overcome slopes up to 60°. The absence of complete vertical movement in these designs may limit the mobility of the robots inside the colon, which comprises both ascending and descending sections. The robot by Manfredi et al. [16] has the capability to climb upward and anchor, however, its speed is constrained by the chosen locomotion strategy. In contrast, our robot design offers the ability to ascend in dry deformable environments with good velocity, thanks to the incorporation of an asymmetrically supporting balloon. This feature enables the robot to climb upward within the colon. In addition, in terms of locomotion in simulated human colons, our robot can traverse a phantom colon that includes ascending, descending, and turning sections. Previous studies primarily focused on horizontal arrangements of the simulated route, which may not accurately reflect the complexities of the colon environment. However, our robot cannot traverse on colon

TABLE VI
CHARACTERISTICS OF COLONOSCOPY ROBOTS

Ref	Locomotion Method	Anchoring Method	Slope Overcoming Capability (Environment)	Velocity (mm/s)
[26]	Worm-driven caterpillars	None	60° (excised porcine colon)	5.0±4.0 (0.038 BL/s)
[17]	Segment bending	Segment bending	None	1.21 (0.002 BL/s)
[16]	Inchworm -like	Balloon	90° (rigid tube)	2.8 (0.047 BL/s)
[27]	Worm-driven treads	None	None	40 (0.67 BL/s)
[52]	Flexible paddles	None	None	6.5 (0.19 BL/s)
[28]	Worm gear-driven tracks	None	45° (acrylic tube)	∼3.5 (0.027 BL/s)
[29]	Magnetic	None	<10° (pig colon)	∼1.47
[30]	Electro -magnetic	None	None	54 (1.13 BL/s)
This work	Wave-like locomotion	Ballon	90° (acrylic tube) None (wet phantom colon)	6.96 (0.03 BL/s) 17.94 (0.076 BL/s)

model with high softness, which may limit the application in real colon.

Furthermore, we introduced the use of training lubricants for colonoscopy, which had not been presented in earlier studies. Although our setup is simplified, this inclusion addresses an important aspect of real-world colonoscopy procedures. In short, even our robots show some potential, but the limitation in locomotion in very soft environment needs to be addressed in order to be applied in real coloscopy.

IX. CONCLUSION

In this research, we proposed the design, fabrication process, and physical model of a self-propelled inspection robot. By utilizing the casting technique, a small-size structure, which is suitable for tasks involving inspecting narrow environments, can be realized. The one-sided tail balloon allows the robot to perform vertical locomotion with litter sliding while retaining smooth and rapid wave-like motion. Two theoretical models were developed to predict the velocity of the robot and the lateral force exerted on the surroundings in the case of horizontal locomotion. Characterization of the robot was conducted with a variety of input parameters and types of workspace to prove the rationality of the models and determine the optimal set of working conditions. The robot could achieve a peak velocity of 40.11 mm/s (0.171 BL/s) in rigid tube and maintain little impact force on the environments, which was less than 1 N. In terms of applications, we present the potential in tube inspection and self-propelled colonoscopes. The robot is capable of traveling through complex layout of a simulation model of human containing both horizontally and vertically in 3 min 14 s. In a simpler arrangement of the phantom colon with the inclusion of training lubricants, the robot achieves an average speed of 17.94 mm/s. In terms of limitation, our design encounters difficulties in traversing environments with extreme softness and low constraints. Therefore, the current robot's configuration and locomotive strategies are well-suited for self-propulsion in cavities of channels with sufficient stiffness and a moderate level of complexity. In future work, we will address the problems mentioned in Section VIII and aim to develop a fully functional robot for real-world applications.

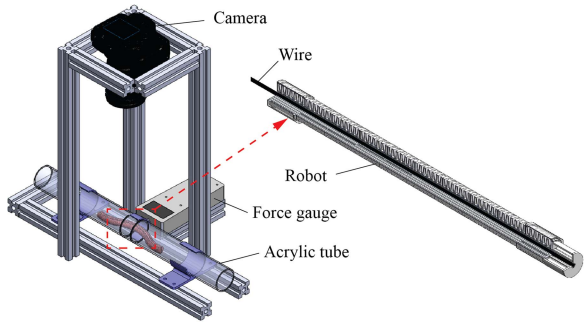

Fig. 13. Experimental setup for the measuring of velocity and lateral force of robot with commercial wire inside.

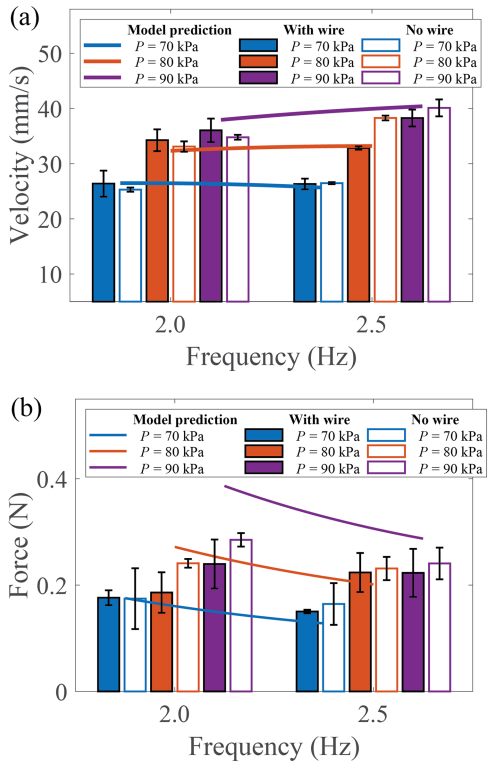

Fig. 14. Results for experiments comparing the robot's performance with a wire inside and with no wire. (a) Experiment of velocity. (b) Experiment of lateral force.

APPENDIX
EFFECT OF CABLE INSIDE ROBOT'S BODY ON THE VELOCITY AND LATERAL FORCE

To verify the effect of a thin and flexible object inserted into the robot, we put a commercial electrical wire with an outer diameter of 1.16 mm and then conducted experiments to evaluate the robot's performance. The experimental setup is shown in Fig. 13, which is similar to the arrangement presented in Section V. The robot performs locomotion in a 500 mm long acrylic tube, while a camera is placed above to record the experiment.

A force gauge is attached to the side of the tube to log the force value. The test was conducted with the input pressure of (70, 80, 90 kPa) and frequency of (2.0, 2.5 Hz). As seen in Fig. 14, there is little difference between the performances of the robot with and without the wire. The average deviation in velocity is 1.82 mm/s, while the average difference for lateral force is 0.02 N. The results prove that in the case of housing a very thin and flexible wire, the working of the robot is not considerably affected, and the evaluations of the analytical models presented in the article still retain their validity.

Acknowledgment

The authors would like to thank Mr. Le Dinh Minh Nhat for his technical support and Dr. Bui Tien Son for his advice on modeling and experimental data processing. The authors would also like to thank Dr. David Price for his proofreading of this manuscript. We also would like to thank the Editorial Board (Editor, Associate Editor) and anonymous reviewers for their valuable comments and suggestions for improving the quality of this article.

References

[1] S. Kim, C. Laschi, and B. Trimmer, "Soft robotics: A bioinspired evolution in robotics," *Trends Biotechnol.*, vol. 31, no. 5, pp. 287–294, 2013.
[2] A. Crespi, K. Karakasiliotis, A. Guignard, and A. J. Ijspeert, "Salamandra robotica II: An amphibious robot to study salamander-like swimming and walking gaits," *IEEE Trans. Robot.*, vol. 29, no. 2, pp. 308–320, Apr. 2013.
[3] A. Crespi and A. J. Ijspeert, "Online optimization of swimming and crawling in an amphibious snake robot," *IEEE Trans. Robot.*, vol. 24, no. 1, pp. 75–87, Feb. 2008.
[4] C. Wang, V. R. Puranam, S. Misra, and V. K. Venkiteswaran, "A snake-inspired multi-segmented magnetic soft robot towards medical applications," *IEEE Robot. Automat. Lett.*, vol. 7, no. 2, pp. 5795–5802, Apr. 2022.
[5] L. Manfredi et al., "A bioinspired autonomous swimming robot as a tool for studying goal-directed locomotion," *Biol. Cybern.*, vol. 107, no. 5, pp. 513–527, 2013.
[6] D. Q. Nguyen and V. A. Ho, "Anguilliform swimming performance of an eel-inspired soft robot," *Soft Robot.*, vol. 9, no. 3, pp. 425–439, 2022.
[7] A. A. Transeth, R. I. Leine, C. Glocker, K. Y. Pettersen, and P. Liljebäck, "Snake robot obstacle-aided locomotion: Modeling, simulations, and experiments," *IEEE Trans. Robot.*, vol. 24, no. 1, pp. 88–104, Feb. 2008.
[8] T. Takemori, M. Tanaka, and F. Matsuno, "Ladder climbing with a snake robot," in *Proc. IEEE/RSJ Int. Conf. Intell. Robots Syst.*, 2018, pp. 1–9.
[9] F. Richter, P. V. Gavrilov, H. M. Lam, A. Degani, and M. C. Yip, "Arcsnake: Reconfigurable snakelike robot with archimedean screw propulsion for multidomain mobility," *IEEE Trans. Robot.*, vol. 38, no. 2, pp. 797–809, Apr. 2022.
[10] Y. Zhang, D. Yang, P. Yan, P. Zhou, J. Zou, and G. Gu, "Inchworm inspired multimodal soft robots with crawling, climbing, and transitioning locomotion," *IEEE Trans. Robot.*, vol. 38, no. 3, pp. 1806–1819, Jun. 2021.
[11] H. Omori, T. Hayakawa, and T. Nakamura, "Locomotion and turning patterns of a peristaltic crawling earthworm robot composed of flexible units," in *Proc. IEEE/RSJ Int. Conf. Intell. Robots Syst.*, 2008, pp. 1630–1635.
[12] X. Zhang, T. Pan, H. L. Heung, P. W. Y. Chiu, and Z. Li, "A biomimetic soft robot for inspecting pipeline with significant diameter variation," in *Proc. IEEE/RSJ Int. Conf. Intell. Robots Syst.*, 2018, pp. 7486–7491.
[13] B. Zhang, Y. Fan, P. Yang, T. Cao, and H. Liao, "Worm-like soft robot for complicated tubular environments," *Soft Robot.*, vol. 6, no. 3, pp. 399–413, 2019.
[14] X. Liu, M. Song, Y. Fang, Y. Zhao, and C. Cao, "Worm-inspired soft robots enable adaptable pipeline and tunnel inspection," *Adv. Intell. Syst.*, vol. 4, no. 1, 2022, Art. no. 2100128.
[15] Y. Lin, Y.-X. Xu, and J.-Y. Juang, "Single-actuator soft robot for in-pipe crawling," *Soft Robot.*, vol. 10, no. 1, pp. 174–186, 2022.
[16] L. Manfredi, E. Capoccia, G. Ciuti, and A. Cuschieri, "A soft pneumatic inchworm double balloon (spid) for colonoscopy," *Sci. Rep.*, vol. 9, no. 1, pp. 1–9, 2019.
[17] J. E. Bernth, A. Arezzo, and H. Liu, "A novel robotic meshworm with segment-bending anchoring for colonoscopy," *IEEE Robot. Autom. Lett.*, vol. 2, no. 3, pp. 1718–1724, Jul. 2017.
[18] X. Qi, H. Shi, T. Pinto, and X. Tan, "A novel pneumatic soft snake robot using traveling-wave locomotion in constrained environments," *IEEE Robot. Autom. Lett.*, vol. 5, no. 2, pp. 1610–1617, Apr. 2020.
[19] S.-g. Roh and H. R. Choi, "Differential-drive in-pipe robot for moving inside urban gas pipelines," *IEEE Trans. Robot.*, vol. 21, no. 1, pp. 1–17, Feb. 2005.
[20] T. Oya and T. Okada, "Development of a steerable, wheel-type, in-pipe robot and its path planning," *Adv. Robot.*, vol. 19, no. 6, pp. 635–650, 2005.
[21] T. Baba, Y. Kameyama, T. Kamegawa, and A. Gofuku, "A snake robot propelling inside of a pipe with helical rolling motion," in *Proc. SICE Annu. Conf.*, 2010, pp. 2319–2325.
[22] S. A. Fjerdingen, P. Liljebäck, and A. A. Transeth, "A snake-like robot for internal inspection of complex pipe structures (piko)," in *2009 IEEE/RSJ Int. Conf. Intell. Robots Syst.*, 2009, pp. 5665–5671.
[23] K.-H. Yoon and Y.-W. Park, "Pipe inspection robot actuated by using compressed air," in *2010 IEEE/ASME Int. Conf. Adv. Intell. Mechatron.*, 2010, pp. 1345–1349.
[24] Y.-S. Kwon, B. Lee, I.-C. Whang, and B.-J. Yi, "A pipeline inspection robot with a linkage type mechanical clutch," in *2010 IEEE/RSJ Int. Conf. Intell. Robots Syst.*, 2010, pp. 2850–2855.
[25] X. Yu, Y. Chen, M. Z. Chen, and J. Lam, "Development of a novel in-pipe walking robot," in *2015 IEEE Int. Conf. Inf. Autom.*, 2015, pp. 364–368.
[26] D. Lee, S. Joe, J. Choi, B.-I. Lee, and B. Kim, "An elastic caterpillar-based self-propelled robotic colonoscope with high safety and mobility," *Mechatronics*, vol. 39, pp. 54–62, 2016.
[27] G. A. Formosa, J. M. Prendergast, S. A. Edmundowicz, and M. E. Rentschler, "Novel optimization-based design and surgical evaluation of a treaded robotic capsule colonoscope," *IEEE Trans. Robot.*, vol. 36, no. 2, pp. 545–552, Apr. 2020.
[28] V. Consumi, L. Lindenroth, J. Merlin, D. Stoyanov, and A. Stilli, "Design and evaluation of the softscreen capsule for colonoscopy," *IEEE Robot. Autom. Lett.*, vol. 8, no. 3, pp. 1659–1666, Mar. 2023.
[29] J. W. Martin et al., "Enabling the future of colonoscopy with intelligent and autonomous magnetic manipulation," *Nature Mach. Intell.*, vol. 2, no. 10, pp. 595–606, 2020.
[30] J. Zhang, Y. Liu, J. Tian, D. Zhu, and S. Prasad, "Design and experimental investigation of a vibro-impact capsule robot for colonoscopy," *IEEE Robot. Autom. Lett.*, vol. 8, no. 3, pp. 1842–1849, Mar. 2023.
[31] D. Rus and M. T. Tolley, "Design, fabrication and control of soft robots," *Nature*, vol. 521, no. 7553, pp. 467–475, 2015.
[32] D. Q. Nguyen et al., "Kinematic evaluation of a series of soft actuators in designing an eel-inspired robot," in *Proc. IEEE/SICE Int. Symp. Syst. Integration*, 2020, pp. 1288–1293.
[33] A. A. Transeth, R. I. Leine, C. Glocker, and K. Y. Pettersen, "3-D snake robot motion: Nonsmooth modeling, simulations, and experiments," *IEEE Trans. Robot.*, vol. 24, no. 2, pp. 361–376, Apr. 2008.
[34] P. Liljebäck, K. Y. Pettersen, Ø. Stavdahl, and J. T. Gravdahl, "A simplified model of planar snake robot locomotion," in *Proc. IEEE/RSJ Int. Conf. Intell. Robots Syst.*, 2010, pp. 2868–2875.
[35] A. Akbarzadeh and H. Kalani, "Design and modeling of a snake robot based on worm-like locomotion," *Adv. Robot.*, vol. 26, no. 5–6, pp. 537–560, 2012.
[36] C. D. Onal and D. Rus, "Autonomous undulatory serpentine locomotion utilizing body dynamics of a fluidic soft robot," *Bioinspiration Biomimetics*, vol. 8, no. 2, 2013, Art. no. 026003.
[37] M. Luo, M. Agheli, and C.D. Onal, "Theoretical modeling and experimental analysis of a pressure-operated soft robotic snake," *Soft Robot.*, vol. 1, no. 2, pp. 136–146, 2014.
[38] R. Ariizumi and F. Matsuno, "Dynamic analysis of three snake robot gaits," *IEEE Trans. Robot.*, vol. 33, no. 5, pp. 1075–1087, Oct. 2017.
[39] W. Zhao, J. Wang, and Y. Fei, "A multigait continuous flexible snake robot for locomotion in complex terrain," *IEEE/ASME Trans. Mechatron.*, vol. 27, no. 5, pp. 3751–3761, Oct. 2022.
[40] L. Li et al., "Generation of efficient rectilinear gait based on dynamic morphological computation and its theoretical analysis," *IEEE Robot. Autom. Lett.*, vol. 6, no. 2, pp. 841–848, Apr. 2021.
[41] H. Niu et al., "Magworm: A biomimetic magnet embedded worm-like soft robot," *Soft Robot.*, vol. 8, no. 5, pp. 507–518, 2021.
[42] Z. Wang and S. Hirai, "Soft gripper dynamics using a line-segment model with an optimization-based parameter identification method," *IEEE Robot. Autom. Lett.*, vol. 2, no. 2, pp. 624–631, Apr. 2017.

[43] D. Massalou, C. Masson, S. Afquir, P. Baqué, P.-J. Arnoux, and T. Bège, "Mechanical effects of load speed on the human colon," *J. Biomech.*, vol. 91, pp. 102–108, 2019.
[44] M. Finocchiaro et al., "Physical simulator for colonoscopy: A modular design approach and validation," *IEEE Access*, vol. 11, pp. 36945–36960, 2023.
[45] X. Yang, Q. Wei, C. Zhang, K. Zhou, L. Kong, and W. Jiang, "Colon polyp detection and segmentation based on improved MRCNN," *IEEE Trans. Instrum. Meas.*, vol. 70, 2021, Art no. 4501710.
[46] K. B. Ozyoruk et al., "Endoslam dataset and an unsupervised monocular visual odometry and depth estimation approach for endoscopic videos," *Med. Image Anal.*, vol. 71, 2021, Art. no. 102058.
[47] H. Kim, O. C. Kara, and F. Alambeigi, "A soft and inflatable vision-based tactile sensor for inspection of constrained and confined spaces," *IEEE Sensors J.*, vol. 23, no. 23, pp. 29605–29618, Dec. 2023.
[48] M. N. Appleyard, C. A. Mosse, T. N. Mills, G. D. Bell, F. D. Castillo, and C. P. Swain, "The measurement of forces exerted during colonoscopy," *Gastrointestinal Endoscopy*, vol. 52, no. 2, pp. 237–240, 2000.
[49] S. Johnson, M. Schultz, M. Scholze, T. Smith, J. Woodfield, and N. Hammer, "How much force is required to perforate a colon during colonoscopy? An experimental study," *J. Mech. Behav. Biomed. Mater.*, vol. 91, pp. 139–148, 2019.
[50] S. Dogramadzi, G. Virk, G. Bell, R. Rowland, and J. Hancock, "Recording forces exerted on the bowel wall during colonoscopy: In vitro evaluation," *Int. J. Med. Robot. Comput. Assist. Surg.: MRCAS*, vol. 1, pp. 89–97, 2005.
[51] M. McCandless, A. Gerald, A. Carroll, H. Aihara, and S. Russo, "A soft robotic sleeve for safer colonoscopy procedures," *IEEE Robot. Autom. Lett.*, vol. 6, no. 3, pp. 5292–5299, Jul. 2021.
[52] K. Osawa et al., "Self-propelled colonoscopy robot using flexible paddles," *IEEE Robot. Autom. Lett.*, vol. 5, no. 4, pp. 6710–6716, Oct. 2020.

Tuan Tai Nguyen (Student Member, IEEE) received the B.Eng. degree in mechatronics engineering from Hanoi University of Science and Technology (HUST), Vietnam, in 2020, the master's degree in materials science, in 2023, from Soft Haptics Lab., Japan Advanced Institute of Science and Technology (JAIST), Nomi, Japan, where he is currently working toward the Ph.D. degree in soft continuum robot arm with vision-based tactile sensing and contact-based control (supported by MEXT scholarship).

His research interests are soft robotics, bio-inspired robots, continuum robots, and tactile sensing.

Mr. Nguyen was a recipient of the Outstanding Performance Award for his master's degree at JAIST (2023).

Dinh Quang Nguyen (Member, IEEE) received Degree of Engineer and Master of Science, in the field of mechanical engineering, from the Hanoi University of Science and Technology (HUST), Vietnam, in 2011 and 2013, respectively, and the Ph.D. degree in scalable eel-like robot using series of soft actuators from the School of Materials Science from Japan Institute of Science and Technology (JAIST), Ishikawa, Japan, in 2022 (supported by MEXT Scholarship).

From 2013 to 2018, he worked as a Lecturer with Hanoi University of Industry (HaUI), Vietnam. After graduation, Dr. Nguyen led a laboratory on Simulation and High-Performance Computing (SHPC) at Institute of Technology, HaUI. From 2024, he joined Department of Robotics Engineering, Faculty of Electronics and Telecommunications, University of Engineering and Technology - Vietnam National University (VNU-UET). His research interests are soft robotics, biomimetics, functional materials, and mechanical engineering.

Van Anh Ho (Senior Member, IEEE) received the bachelor's degree in electrical engineering from Hanoi University of Science and Technology, Vietnam, in 2007, and the Master degree in mechanical engineering from Ritsumeikan University, Kyoto, Japan, in 2009, the Ph.D. degree in robotics from Ritsumeikan Unviersity, in 2012.

He completed the JSPS Postdoctoral Fellowship in 2013 before joining Advanced Research Center Mitsubishi Electric Corp., Japan as a Research Scientist. From 2015 to 2017, he worked as an Assistant Professor with Ryukoku University, Kyoto, Japan where he led a laboratory on soft haptics, soft modeling. From 2017, he joined the Japan Advanced Institute of Science and Technology (JAIST) for setting up a laboratory on soft robotics. His current research interests are soft robotics, soft haptic interaction, tactile sensing, grasping and manipulation, bio-inspired robots.

Dr. Ho was a recipient of the prestigious Japan Society for the Promotion of Science (JSPS) Research Fellowship for Young Scientist for his PhD course (DC2) and postdoctoral fellowship. He was the recipient of the 2019 IEEE Nagoya Chapter Young Researcher Award, finalists for Best Paper Awards at Robotics: Science and Systems (RSS 2023), IEEE SII (2024, 2016) and IEEE RoboSoft (2020). He is a member of The Robotics Society of Japan (RSJ). He is serving as an Associate Editor for many international conferences, such as RSS, IROS, ICRA, RoboSoft; as well as for journals such as IEEE TRANSACTIONS FOR ROBOTICS (T-RO), IEEE ROBOTICS AND AUTOMATION LETTERS (RA-L), and Advanced Robotics. He is General Chair of 2024 IEEE/SICE International Symposium on System Integration (SII 2023), and General Chair of SII 2024.